AGU PUBLICATIONS

Geophysical Research Letters

RESEARCH LETTER
10.1002/2016GL071612

Key Points:
- Physical properties of Mercury's cross-tail current sheet are more intense but similar to Earth's
- Inner edge of cross-tail current sheet and mean NMNL location are found to be ~1.2 and −3 R_M
- Stress balance seems to require significant contributions from heavy planetary ions and/or H^+ anisotropy

Correspondence to:
G. Poh,
gangkai@umich.edu

Citation:
Poh, G., J. A. Slavin, X. Jia, J. M. Raines, S. M. Imber, W.-J. Sun, D. J. Gershman, G. A. DiBraccio, K. J. Genestreti, and A. W. Smith (2017), Mercury's cross-tail current sheet: Structure, X-line location and stress balance, *Geophys. Res. Lett.*, *44*, 678–686, doi:10.1002/2016GL071612.

Received 15 OCT 2016
Accepted 22 DEC 2016
Accepted article online 23 DEC 2016
Published online 27 JAN 2017

Mercury's cross-tail current sheet: Structure, X-line location and stress balance

Gangkai Poh[1], James A. Slavin[1], Xianzhe Jia[1], Jim M. Raines[1], Suzanne M. Imber[2], Wei-Jie Sun[3,4], Daniel J. Gershman[5], Gina A. DiBraccio[6], Kevin J. Genestreti[7,8], and Andy W. Smith[9]

[1]Department of Climate and Space Sciences and Engineering, University of Michigan, Ann Arbor, Michigan, USA, [2]Department of Physics and Astronomy, University of Leicester, Leicester, UK, [3]Key Laboratory of Earth and Planetary Physics, Institute of Geology and Geophysics, Chinese Academy of Sciences, Beijing, China, [4]School of Earth and Space Sciences, Peking University, Beijing, China, [5]Heliophysics Science Division, NASA Goddard Space Flight Center, Greenbelt, Maryland, USA, [6]Solar System Exploration Division, NASA Goddard Space Flight Center, Greenbelt, Maryland, USA, [7]Department of Physics and Astronomy, University of Texas at San Antonio, San Antonio, Texas, USA, [8]Space Science and Engineering Division, Southwest Research Institute, San Antonio, Texas, USA, [9]Department of Physics and Astronomy, University of Southampton, Southampton, UK

Abstract The structure, X-line location, and magnetohydrodynamic (MHD) stress balance of Mercury's magnetotail were examined between $-2.6 < X_{MSM} < -1.4$ R_M using MErcury Surface, Space ENvironment, GEochemistry, and Ranging (MESSENGER) measurements from 319 central plasma sheet (CPS) crossings. The mean plasma β in the CPS calculated from MESSENGER data is ~ 6. The CPS magnetic field was southward (i.e., tailward of X-line) ~ 2–18% of the time. Extrapolation of downtail variations in B_Z indicates an average X-line location at −3 R_M. Modeling of magnetic field measurements produced a cross-tail current sheet (CS) thickness, current density, and inner CS edge location of 0.39 R_M, 92 nA/m^2 and −1.22 R_M, respectively. Application of MHD stress balance suggests that heavy planetary ions may be important in maintaining stress balance within Mercury's CPS. Qualitative similarities between Mercury's and Earth's magnetotail are remarkable given the differences in upstream conditions, internal plasma composition, finite gyro-radius scaling, and Mercury's lack of ionosphere.

1. Introduction

The dominant process transferring solar wind energy into Mercury's magnetosphere is magnetic reconnection at the dayside magnetopause [*Slavin et al*., 2009; *DiBraccio et al*., 2013]. Following dayside reconnection, opened magnetic flux is transported antisunward by the flow of the solar wind, forming a magnetotail with two open magnetic field regions, i.e., the two tail lobes. These open field lines have one end connected to the planetary magnetic field and the other to the interplanetary magnetic field (IMF). The northern and southern tail lobes contain fields oriented in opposite directions. Separating the two tail lobes is the higher β (i.e., ratio of plasma thermal to magnetic pressure) and closed field line region known as the plasma sheet. Between each tail lobe and the plasma sheet is a region of lower β (~ 0.1 at Earth [*Baumjohann et al*., 1988]) flux tubes recently "closed" by magnetic reconnection known as the plasma sheet boundary layer (PSBL). The CPS layer contains an embedded cross-tail current, which flows in the dawn-to-dusk direction [*Rich et al*., 1972]. The crossing of a CPS is identified by the reversal of the sunward/antisunward component of the magnetic field and a decrease in the magnitude $|\mathbf{B}|$. Due to the weak magnetic field and presence of hot, dense plasma, β is typically $>>1$ in Mercury's CPS [*Gershman et al*., 2014; *Raines et al*., 2011].

The MErcury Surface, Space ENvironment, GEochemistry, and Ranging (MESSENGER) spacecraft conducted three flybys of Mercury before it became the first spacecraft to orbit Mercury on 18 March 2011. During these flybys, MESSENGER sampled Mercury's magnetotail at downtail distances up to 3 R_M away from Mercury and provided an opportunity to characterize the structure and dynamics of the magnetotail. Initial analysis of MESSENGER flybys data [*Slavin et al*., 2010; *Slavin et al*., 2012a] has shown that Mercury's magnetotail is highly variable with timescales of seconds to minutes, which is consistent with the high magnetopause reconnection rates that had been predicted for Mercury [*Slavin and Holzer*, 1979]. MESSENGER observed relatively large magnetic field component normal to the magnetopause [*DiBraccio et al*., 2013] and showers of large flux transfer events [*Slavin et al*., 2012b; *Imber et al*., 2014], which are indicative of high magnetopause

reconnection activity, increase the tail magnetic flux content by up to a factor of 2 [*Slavin et al*., 2010; *Slavin et al*., 2012a] via the Dungey cycle [*Dungey*, 1961] at Mercury. This intense loading of magnetic flux in the lobes increases the overall flaring of the nightside magnetopause and enhances the solar wind pressure exerted on the magnetotail. These pressure enhancements lead to thinning of the cross-tail CS and tail reconnection. Observations of plasmoids [*DiBraccio et al*., 2015; *Slavin et al*., 2012a; *Sun et al*., 2016], dipolarizations [*Sundberg et al*., 2012], and substorms [*Slavin et al*., 2010; *Sun et al*., 2015] strongly support the rapid dissipation of magnetotail energy through magnetic reconnection in a manner similar to that observed at Earth [*Sharma et al*., 2008]. MESSENGER's orbit around Mercury provided continuous magnetic field [*Anderson et al*., 2007] and plasma ion [*Andrews et al*., 2007] measurements, which allow the large-scale structure in Mercury's magnetotail to be characterized. Here we examine the structure, X-line location, and MHD stress balance in Mercury's magnetotail.

2. MESSENGER Instrumentation and Tail Current Sheet Crossing Identification

In this study, we utilize the full-resolution data from MESSENGER's Magnetometer (MAG) (20 vectors/s) and Fast Imaging Plasma Spectrometer (FIPS) (one energy scan per 10 s). Figure 1a shows MESSENGER's magnetic field observations during a traversal of Mercury's cross-tail CS on 3 February 2013 in the aberrated Mercury solar magnetospheric (MSM) coordinate system. The MSM system is centered on Mercury's offset internal dipole [*Alexeev et al*., 2010; *Anderson et al*., 2011], the X and Z axes are sunward and parallel to the planetary spin axis, respectively. The Y axis completes the right-handed system. We accounted for the aberration effect (i.e., orbital motion of Mercury with respect to the solar wind) by rotating the MSM X and Y axes such that X' is opposite to the solar wind velocity vector and corresponds to the central axis of the magnetotail. The rotation angle was calculated using daily averages of Mercury's orbital motion and an assumed radial solar wind velocity of 400 km/s. In Figure 1, the spacecraft first encountered the southern lobe, characterized by the strong, low-variance magnetic fields of ~60 nT, predominantly oriented in the negative $B_{X'}$ direction. The PSBL (yellow) was identified by small decreases in $|\mathbf{B}|$ (~10%) and moderate fluctuations of ~20 nT as compared to the lobe field [*Slavin et al*., 1985]. The spacecraft then entered the CPS (red) characterized by a further decrease in the $|\mathbf{B}|$ and reversal of $B_{X'}$ across the magnetotail current layer. Lastly, MESSENGER entered the northern lobe when $|\mathbf{B}|$ increased back to 60 nT with low levels of fluctuations in $|\mathbf{B}|$. Before exiting into the northern lobe, MESSENGER observed two large-scale CS oscillations or flapping motions (i.e., fluctuations in $B_{X'}$, which are common in planetary magnetotails [see *Volwerk et al*., 2013].

We surveyed 4 years of MESSENGER's MAG data and identified a total of 319 CPS crossings based on the following selection requirements:

1. Well-defined boundary between the moderately fluctuating magnetic field intensity in the PSBL and the highly fluctuating, large decrease in magnetic field intensity in the CPS.
2. Clear reversal of B_X embedded in the CPS corresponding to the cross-tail CS.
3. Average $|\mathbf{B}|$ in the CPS must be less than 50% of the $|\mathbf{B}|$ lobe averaged over the lobe interval during individual traversal.

The locations of each of the CPS crossings identified in this study are plotted in Figure 1b in the equatorial $\left(X'_{\mathrm{MSM}} - Y'_{\mathrm{MSM}}\right)$ and meridional $\left(X'_{\mathrm{MSM}} - Z'_{\mathrm{MSM}}\right)$ planes along with the T96-modeled magnetic field lines [*Tsyganenko and Stern*, 1996] scaled to the size of Mercury's magnetosphere by dividing with a factor of 8 [*Ogilvie et al*., 1977]. The CPS crossings were evenly distributed around midnight $\left(Y'_{\mathrm{MSM}} \sim 0\right)$ and covered a range of downtail distances from −1.1 to −3.0 R_{M}.

3. Analysis

3.1. Downtail Variation of CPS and Lobe Magnetic Field

We examined the variation of the magnetic field intensity in the lobe (B_{lobe}) and CPS (B_{CPS}) as a function of downtail distances (i.e., X'_{MSM}). Using MESSENGER's (MSGR) and Mariner 10's (M10) flyby magnetic field data, *Slavin et al*. [2012a] showed that a power law relation can be used to describe the decrease in B_{lobe} with X'_{MSM} due to the decrease in flaring of the magnetotail as it becomes more cylindrical:

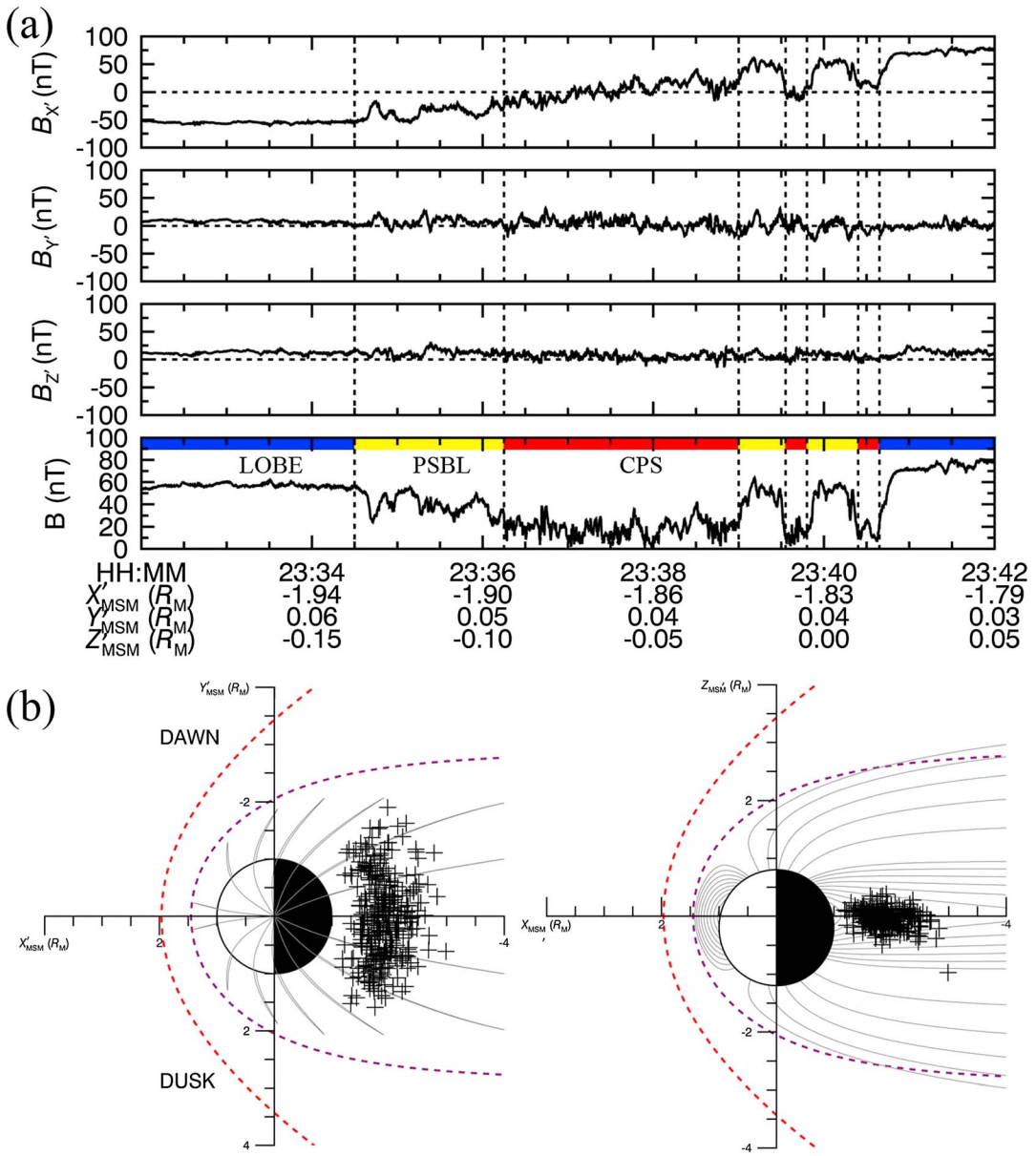

Figure 1. (a) Full-resolution MESSENGER magnetic field measurements on 3 February 2013. (b) Average positions of each CS crossing in the (left) equatorial and (right) meridional plane. Model bow shock (BS) and magnetopause (MP) from *Winslow et al.* [2013] are shown.

$$|B_{\text{lobe}}|\left(\left|X'_{\text{MSM}}\right|\right) = A\left|X'_{\text{MSM}}\right|^{G} + B_0 \tag{1}$$

where A is the scaling constant, G is the power law exponent, and B_0 is the asymptotic magnetic field. The MSGR $<B_{\text{lobe}}>$ values are averaged in 0.1 R_M bins along X'_{MSM} for the entire orbital phase and displayed in Figure 2a. Our result shows that B_{lobe} falls off with $G \sim 3.1 \pm 0.1$ and has an asymptotic value of $B_0 \sim 41.4 \pm 1.4$ nT. The fitted curve suggests that lobe flaring ceases near $X'_{\text{MSM}} \sim -3.5$ R_M, where B_{lobe} becomes constant. Figure 2b shows the MSGR $<B_{\text{CPS}}>$ for orbital phase as a function of X'_{MSM}, where all measured B_{CPS} values are averaged in 0.1 R_M bins. Our results show that $<B_{\text{CPS}}>$ decreases with $G \sim -8.9 \pm 0.1$ and asymptotes at $X'_{\text{MSM}} \sim -1.8$ R_M with $B_0 \sim 16.6 \pm 0.7$ nT. As compared to *Slavin et al.* [2012a] earlier analysis of Mercury's CPS during the first flyby (M1) when the IMF was northward, our observation of weaker magnetic field is attributed to the presence of a denser and hotter plasma sheet. In fact, assuming pressure balance

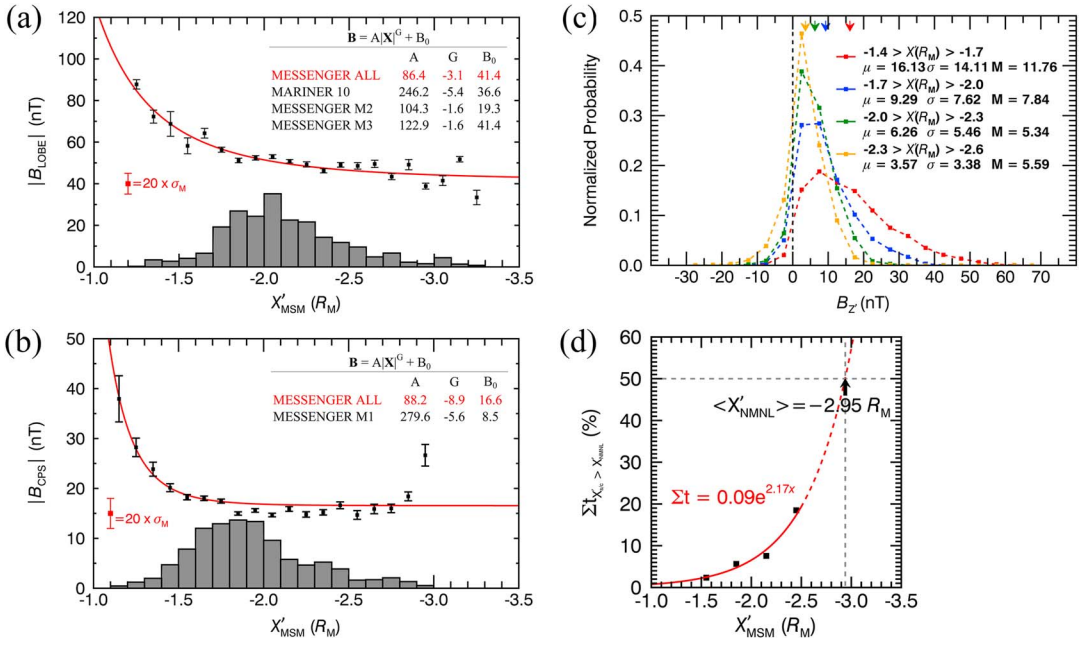

Figure 2. (a) B_{lobe} and (b) B_{CPS} as a function of X'_{MSM}. A power law relation was fitted to the data points (red line) with fitting coefficients shown in the table. The histogram for number of data points in each bin is also shown. (c) Normalized probability distributions of B_Z for four downtail regions and the colored arrows represent the mean of each respective distribution. (d) Σt as a function of X'_{MSM}. An exponential relation (red line) is fitted to the data points.

between the lobe and CPS, we can derive an equation for the CPS $\beta = \left[\left(\frac{B^2_{lobe}}{B^2_{CPS}}\right) - 1\right]$. The asymptotic lobe and CPS field intensities determined earlier imply an average value of $\beta \sim 5.2$. This agrees with our calculated β of ~6.5 using FIPS measurements (not shown here).

The normalized probability distribution of B_Z in Figure 2c is derived by binning all measurements into 5 nT bins of B_Z, four X'_{MSM} ranges between −1.4 and −2.6 R_M at intervals of 0.3 R_M, and within ±0.4 R_M away from $Y'_{MSM} = 0$. In a two-dimensional geometry of the X-line, the two antiparallel lobe fields reconnect to form closed (open) magnetic field lines which move sunward (antisunward) at the local Alfvén speed. The closed, sunward (open, antisunward) moving magnetic field line has a positive (negative) B_Z polarity. Figure 2c shows that B_Z is predominantly positive for all X'_{MSM} ranges and the $<B_Z>$ of the distributions decreases with increasing X'_{MSM}. Therefore, we can conclude that MESSENGER crosses the CPS slightly planetward of the statistical X-line, also known as the Near Mercury Neutral Line (NMNL), most of the time. Not shown here, the mean of all measured B_Z measurements is ~9.5 nT.

The probability distribution in Figure 2c also shows that MESSENGER spent ~2% of the CPS crossing occurred tailward of the X-line ($B_Z < 0$). As X'_{MSM} decreases, the time MESSENGER spent tailward of the X-line also increases. At the furthest downtail region ($-2.3 < X'_{MSM}$ (R_M) < -2.6), MESSENGER spend ~18% of its CPS crossing time tailward of the X-line. Figure 2d shows the relationship between the percentage time MESSENGER spent tailward of the X-line (Σt) and X'_{MSM}. We fit the data using an exponential function and estimated the statistical location of the NMNL (i.e., $\Sigma t = 50\%$) to be $X'_{MSM} \sim -2.95\ R_M$.

3.2. Harris Current Sheet Modeling

Due to MESSENGER's highly inclined (~80°) orbit, the spacecraft trajectories through the cross-tail CS are expected to be nearly normal to the tail current sheet on average. The Harris current sheet model [*Harris*, 1962] is the one-dimensional equilibrium solution to the Maxwell-Vlasov equation that describes the planetary magnetotail magnetic field structure in the Z'_{MSM} direction. It has been used extensively in magnetotail

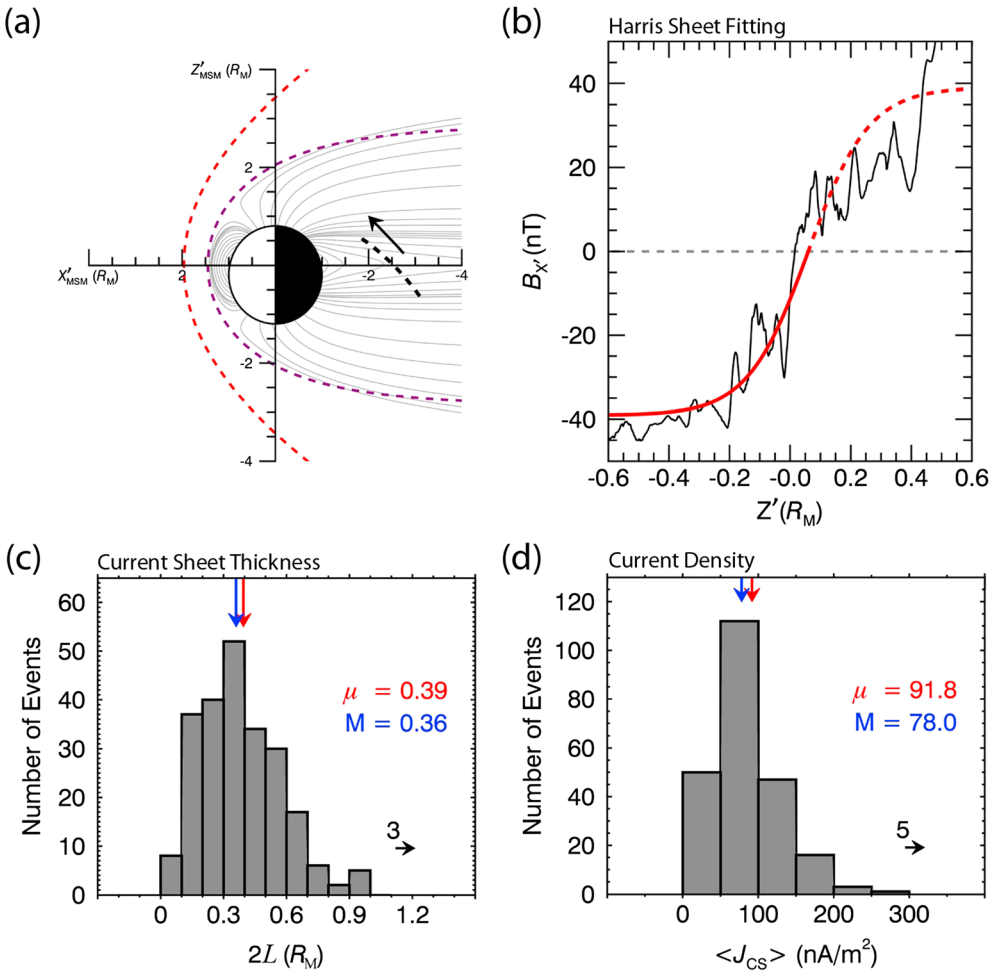

Figure 3. (a) Meridional view of MESSENGER crossing of the cross-tail CS on 23 August 2011. Arrow denotes the spacecraft traveling direction. (b) B_X measurements as a function of Z'_{MSM}. A Harris CS model is fitted to the smoothed data. Histograms of (c) $2L$ and (d) J_{CS} calculated from Harris model fits. The μ and M represent mean and median of the distribution, respectively.

studies by Cluster [e.g., *Nakamura et al.*, 2002; *Narita et al.*, 2013] and reconnection simulations [e.g., *Birn et al.*, 2001]. The relationship between B_X and the cross-tail current density (J_Y) is given by

$$B_X(z) = B_0 \tanh\left(\frac{z - z_0}{L}\right) \tag{2}$$

$$J_Y(z) = \frac{B_0}{\mu_0 L} \mathrm{sech}^2\left(\frac{z - z_0}{L}\right) \tag{3}$$

where B_0 is the asymptotic lobe field, z_0 is the north-south position of the CS center, and L is the characteristic half-thickness of the CS. These are free parameters, which we determined by a least squares fitting procedure of the Harris model to the magnetic field measurements.

Figure 3a shows MESSENGER's trajectory across the cross-tail CS on 23 August 2011 in the meridional plane. Due to the high-latitude (~60°) periapsis of its orbit, MESSENGER moved rapidly toward Mercury at high northern latitudes, as it leaves the CPS, and the dipole magnetic field becomes dominant. For this reason, the fitting procedure is performed only for the southern half of the CS (i.e., $B_X < 0$). To remove the high-frequency B_X fluctuations common to Mercury's CPS, 40 s sliding boxcar averages of the magnetic field are used to low-pass filter the data prior to fitting. Figure 3b shows the averaged B_X measurements (black) and the Harris model result (red) for the 23 August 2011 CPS crossing as a function of Z'_{MSM}. The normalized chi-square χ^2 for this fit is 0.005. This event meets the requirement of $\chi^2 \leq 0.01$ that we have set for acceptable

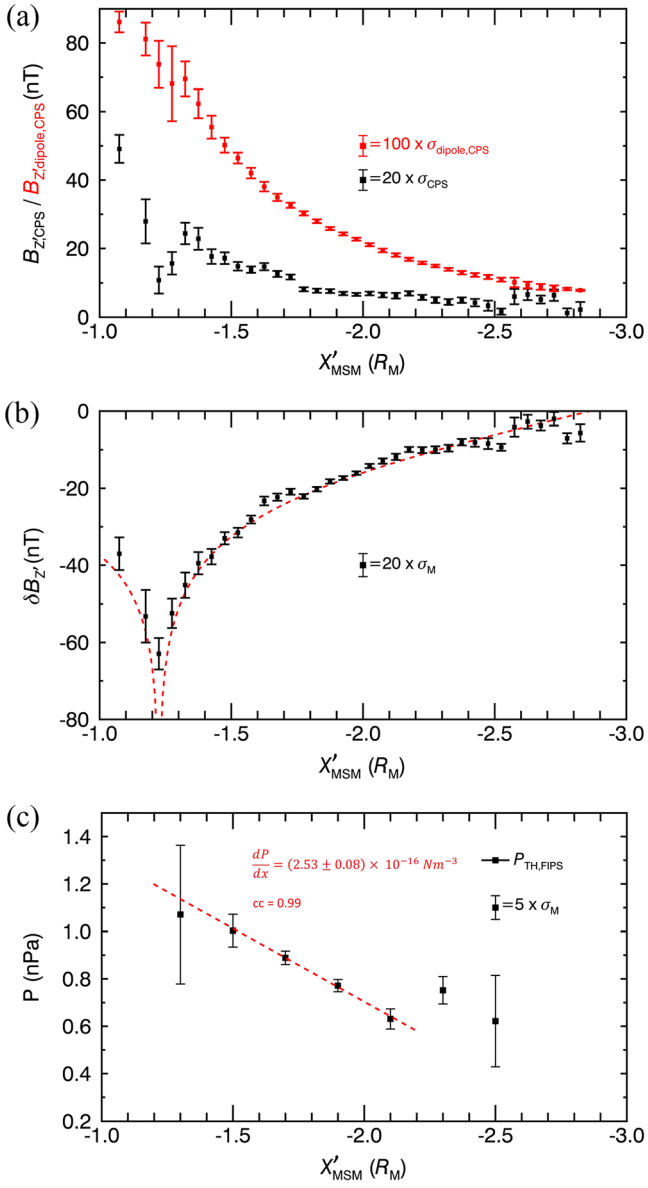

Figure 4. (a) Magnitude of measured B_Z and dipole magnetic field in the CPS and (b) δB_Z as a function of X'_{MSM}. (c) $P_{th,FIPS}$ as a function of X_{MSM}.

fits. Out of the 319 cross-tail CS crossings identified in this study, 234 (~73%) were found to fit the Harris model with $\chi^2 \leq 0.01$. The high percentage of successful model fits suggests that the longer-wavelength structure of Mercury's cross-tail CS is usually well represented by a Harris-type CS. Figures 3c and 3d show the distribution of full thickness ($2L$) and current density averaged over each CS crossing (J_{CS}) calculated from the Harris fitting procedure, respectively. Our analysis indicates that Mercury's CS has a mean $<2L>$ and $<J_{CS}>$ of ~0.39 R_M and ~92 nA/m^2, respectively.

3.3. Downtail Variation of B_Z and Plasma Pressure in the Central Plasma Sheet

We also examined how B_Z in the CPS varies with X'_{MSM}. The measured B_Z in the CPS can be modeled as a superposition of Mercury's intrinsic northward dipole field ($B_{Z,DIPOLE}$), magnetic field perturbations due to the cross-tail CS (δB_Z), and the contribution from Chapman-Ferraro current on the magnetopause surface ($B_{Z,CF}$). $B_{Z,CF}$ decreases approximately as 1/r away from the magnetopause surface. With a total current of ~10^5 A, we estimate that $B_{Z,CF}$ is only ~1–4 nT in the CPS, which is negligible as compared to $B_{Z,DIPOLE}$ or δB_Z. Hence, the $B_{Z,CF}$ term is ignored in our calculations.

The B_Z and $B_{Z,DIPOLE}$ as a function of X'_{MSM} are shown in Figure 4a. We calculated δB_Z by subtracting $B_{Z,DIPOLE}$ from B_Z as a function of X'_{MSM} as shown in Figure 4b. These data show a distinct local minimum at $X'_{MSM} \sim -1.22$ R_M. This minimum corresponds to the inner edge of the CS, where the southward magnetic field perturbation from the CS is the strongest and decreases exponentially sunward from this point. We also calculated the magnetic field perturbation of a two-dimensional semi-infinite CS slab model (red line) with thickness and uniform current density of ~0.39 R_M and 78 nA/m^2 taken from our fitting of the Harris model to the magnetic field profiles measured across the CS. The locations of the inner and outer edge of the CS slab model are free parameters in the least squares fitting between $X'_{MSM} \sim -1.05$ to -2.85 R_M. The outer edge of the CS slab model is ~ -4.5 R_M. We used the median, instead of the mean, of the current density distribution in this slab model since the median is a more accurate measure of the true distribution due to the presence of outliers (events with high current density).

We also determined the downtail variation of the thermal plasma pressure in the CPS using the FIPS H^+ plasma data ($P_{th,FIPS}$). In this manner, the H^+ density (n) and temperature (T) were determined with ~1 min resolution and used to compute $<P_{th,FIPS}>$for each CPS crossing. The values were used to determine the

downtail variation as shown in Figure 4c. The downtail profile of $P_{th,FIPS}$ is similar to that of $|B_{lobe}|^2$, which is expected when the CPS plasma thermal pressure is balanced by the lobe magnetic pressure. To determine the global stress balance of Mercury's CPS, we approximate, to zero order, the downtail profile of $P_{th,FIPS}$ between $X'_{MSM} = -1.2$ and -2.2 R_M to be linear. It was found that $<P_{th,FIPS}>$ decreases linearly at a rate of $\sim 0.62 \pm 0.02$ nPa/R_M and reaches a constant value of ~0.7 nPa at $X'_{MSM} \sim -2.0$ R_M.

3.4. Central Plasma Sheet Stress Balance

For an isotropic plasma sheet in static equilibrium (i.e., $\frac{dv}{dt} = 0$), ∇P must be balanced by the magnetic stress ($\boldsymbol{J} \times \boldsymbol{B}$) (i.e., $\nabla P = \boldsymbol{J} \times \boldsymbol{B}$). Given $<J_{CS}> \sim 78$ nA/m^2 and $<B_Z> \sim 9.5$ nT as determined earlier, we estimate the $\langle \boldsymbol{J} \times \boldsymbol{B} \rangle$ stress to be ~ 1.81 nPa/R_M, which is ~ 3 times greater than $\frac{dP_{th}}{dX}$ (~ 0.62 nPa/R_M) determined by FIPS. The discrepancy suggests that pressure gradient in the H^+ ions alone is insufficient to maintain stress balance in the measured magnetic field in Mercury's CPS. This begs the question of whether the pressure gradient contribution from the heavy planetary ions plays an important part in maintaining equilibrium in Mercury's CPS as is the case in Earth's magnetotail [*Kistler et al*., 2005]. *Gershman et al*. [2014] showed that Na^+ ions are present with a number density ~ 10% of the H^+ density. For the heavy planetary ions to play an important role in maintaining equilibrium in Mercury's CPS, the rate of decrease of plasma pressure with X'_{MSM} would have to be greater than that of the protons. *Rich et al*. [1972] showed that pressure anisotropy in the dominant H^+ ion is required in Earth's CPS to maintain stress balance. However, further analyses of the FIPS measurements, which are beyond the scope of this study, are required in order to evaluate the possible role of proton temperature anisotropies in maintaining equilibrium within Mercury's CPS.

4. Discussion and Summary

We have conducted the first comprehensive study of Mercury's central plasma sheet and the embedded cross-tail current sheet using MESSENGER's MAG and FIPS measurements. Results from the analysis of 319 cross-tail CS traversals indicate that the magnetic field profiles are well described using a Harris model, with full CS thickness and mean current density of 0.39 R_M and 92 nA/m^2, respectively. This thickness is in good agreement with earlier results [*Johnson et al*., 2012; *Sun et al*., 2016]. Our current density determination is much higher than at Earth, i.e., ~ 4 to 25 nA/m^2 [*Artemyev et al*., 2011], but it is in good agreement with global MHD simulations of Mercury's magnetosphere [*Jia et al*., 2015].

We also report the first determination of the inner edge of Mercury's CS derived from MESSENGER's magnetic field data. This local minimum in δB_Z indicates that the inner edge of the CS is located at ~ -1.22 R_M. At Earth, the inner edge of the CS is located at $X'_{GSM} \sim 10$–12 R_E during quiet intervals and shifts earthward to ~ 6–7 R_E during active times [*Wang et al*., 2004; *Kalegaev et al*., 2014]. Using the scaling factor of ~ 8, the quiet time location of the inner edge of Mercury's CS based on the Earth value would be ~ 1.25 R_M, which agrees well our MESSENGER results. Determination of the inner edge location is important to better constrain the physical properties of Mercury's CS in empirical [*Alexeev et al*., 2008; *Korth et al*., 2015] and global simulation models [*Trávníček* et al., 2009; *Jia et al*., 2015].

Our statistical analyses of the MESSENGER data show that B_{lobe} decreases with increasing X'_{MSM} with an exponent of ~ 3.1. At Earth, this exponent ranges from ~ 0.9 to 2.7 [*Nakai et al*., 1999], which is lower than our Mercury results. This suggests that magnetotail flaring should cease comparatively closer to Mercury than is the case at Earth. At Earth, the flaring of the lobes is observed to cease at $X_{GSM} \sim -100$ to -120 R_E [*Slavin et al*., 1985]. We would expect flaring of Mercury's lobe to cease at ~ -12 to -15 R_M, which is outside the range of MESSENGER's orbit. Hence, the distance at which the flaring ceases is still an open question, calling for future measurements at $X'_{MSM} < -3$ R_M. The rate of decrease of B_{CPS} was also shown to follow a power law, with an exponent of ~ 8.9. The corresponding rate of decrease in Earth's CPS ranges from ~ 1.14 to 3.36 for different downtail distances [*Nakai et al*., 1999], which is significantly slower than the Mercury values determined here.

Our analysis shows that the $<B_Z>$ in the CS region sampled by MESSENGER is primarily positive, which suggests that the spacecraft spent most of its time crossing the CS planetward of the NMNL. The estimated mean location of the NMNL based upon the rate of decrease in B_Z is ~ -2.95 R_M. The location of the near-Earth neutral line (NENL) had been widely debated within the community due to importance of reconnection onset location in substorm models. Similarly, the location of the NMNL is important in understanding

Mercury's plasma sheet conditions during substorm initiation. The average NENL location has been shown to occur between $X_{GSM} \sim -20$ and -30 R_E [e.g., *Nagai and Machida*, 1998]. A Time History of Events and Macroscale Interaction during Substorms (THEMIS) survey of magnetotail flux ropes and traveling compression regions estimated the NENL to be located closer to -30 R_E during solar minimum [*Imber et al*., 2011]. The location of NMNL is then expected to be ~ -2.5 to -3.8 R_M, which agrees with our estimated NMNL location of -2.95 R_M. Furthermore, *DiBraccio et al*. [2015] and *Slavin et al*. [2012a] estimated the location of the NMNL to be between ~ -2 and -3 R_M based on the spatial distribution of sunward and antisunward flux ropes. Their NMNL location is closer to Mercury, most likely because they were studying intervals of intense reconnection during which X-line is expected to form closer to the planet.

Analysis of $<P_{th}>$ in Mercury's CPS indicated that it decreases linearly with X'_{MSM} between -1.2 and -2.2 R_M at a rate of 0.62 ± 0.02 nPa/R_M. However, this is only ~ 33% of the mean measured $J \times B$ in the CPS (~ 1.81 nPa/R_M). Hence, we find that the pressure gradient from H^+ is insufficient to maintain pressure balance within Mercury's CPS. Contributions from heavy planetary ions and/or H+ temperature anisotropy are necessary, but further analysis of FIPS measurements is beyond the scope of this study.

In summary, we examined the structure of Mercury's magnetotail. We also determined that average NMNL is located at $X'_{MSM} \sim -3$ R_M and heavy ions are important in maintaining stress balance within Mercury's CPS. Investigation has revealed many qualitative similarities between Mercury's and Earth's magnetotail, despite the differences in upstream conditions, internal plasma composition, finite gyro-radius scalings, and Mercury's lack of ionosphere (see review by *Jackman et al*., 2014). MESSENGER's orbit only allows us to directly observe magnetotail structures and processes in Mercury's near-tail region. Hence, to understand the location and nature of the NMNL and related downtail evolution of Mercury's tail structure, observations at $X_{MSM} < -3$ R_M are necessary. Fortunately, this will take place when measurements from the upcoming European Space Agency's Bepi-Columbo mission, which consists of two spacecraft orbiting Mercury at apogees of ~ -1.6 R_M and -5 R_M, become available in the next decade.

Acknowledgments

All data analyzed in this paper are archived with the NASA Planetary Data System. Support was provided by NASA Discovery Data Analysis Program grants NNX15K88G and NNX15AL01G, Heliophysics Supporting Research NNX15AJ68G, Living With a Star NNX16AJ67G, and Solar System Workings Program grant NNX15AH28G to the University of Michigan. D.J.G. and G.A.D. were supported by NASA ROSES grant NNX16AJ05G. G.A.D. was supported by a NASA Postdoctoral Program appointment at the NASA Goddard Space Flight Center, administered by Universities Space Research Association through a contract with NASA. S.M.I. acknowledges the support of the Leverhulme Trust.

References

Alexeev, I. I., E. S. Belenkaya, S. Y. Bobrovnikov, J. A. Slavin, and M. Sarantos (2008), Paraboloid model of Mercury's magnetosphere, *J. Geophys. Res.*, *113*, A12210, doi:10.1029/2008JA013368.

Alexeev, I. I., et al. (2010), Mercury's magnetospheric magnetic field after the first two MESSENGER flybys, *Icarus*, *209*, 23–39, doi:10.1016/j.icarus.2010.01.024.

Anderson, B. J., M. H. Acuña, D. A. Lohr, J. Scheifele, A. Raval, H. Korth, and J. A. Slavin (2007), The magnetometer instrument on MESSENGER, *Space Sci. Rev.*, *131*, 417–450, doi:10.1007/s11214-007-9246-7.

Anderson, B. J., C. L. Johnson, H. Korth, M. E. Purucker, R. M. Winslow, J. A. Slavin, S. C. Solomon, R. L. McNutt Jr., J. M. Raines, and T. H. Zurbuchen (2011), The global magnetic field of Mercury from MESSENGER orbital observations, *Science*, *333*, 1859–1862, doi:10.1126/science.1211001.

Andrews, G. B., et al. (2007), The energetic particle and plasma spectrometer instrument on the MESSENGER spacecraft, *Space Sci. Rev.*, *131*, 523–556, doi:10.1007/s11214-007-9272-5.

Artemyev, A. V., A. A. Petrukovich, R. Nakamura, and L. M. Zelenyi (2011), Cluster statistics of thin current sheets in the Earth magnetotail: Specifics of the dawn flank, proton temperature profiles and electrostatic effects, *J. Geophys. Res.*, *116*, A09233, doi:10.1029/2011JA016801.

Baumjohann, W., G. Paschmann, N. Sckopke, C. A. Cattell, and C. W. Carlson (1988), Average ion moments in the plasma sheet boundary layer, *J. Geophys. Res.*, *93*, 11,507–11,520, doi:10.1029/JA093iA10p11507.

Birn, J., et al. (2001), Geospace Environmental Modeling (GEM) magnetic reconnection challenge, *J. Geophys. Res.*, *106*, 3715–3719, doi:10.1029/1999JA900449.

DiBraccio, G. A., J. A. Slavin, S. A. Boardsen, B. J. Anderson, H. Korth, T. H. Zurbuchen, J. M. Raines, D. N. Baker, R. L. McNutt Jr., and S. C. Solomon (2013), MESSENGER observations of magnetopause structure and dynamics at Mercury, *J. Geophys. Res. Space Physics*, *118*, 997–1008, doi:10.1002/jgra.50123.

DiBraccio, G. A., et al. (2015), MESSENGER observations of flux ropes in Mercury's magnetotail, *Planet. Space Sci.*, *115*, 77–89, doi:10.1016/j.pss.2014.12.016.

Dungey, J. W. (1961), Interplanetary magnetic fields and the auroral zones, *Phys. Rev. Lett.*, *6*, 47–48.

Gershman, D. J., J. A. Slavin, J. M. Raines, T. H. Zurbuchen, B. J. Anderson, H. Korth, D. N. Baker, and S. C. Solomon (2014), Ion kinetic properties in Mercury's pre-midnight plasma sheet, *Geophys. Res. Lett.*, *41*, 5740–5747, doi:10.1002/2014GL060468.

Harris, E. G. (1962), On a plasma sheath separating regions of oppositely directed magnetic field, *Nuovo Cimento*, *23*, 115–121.

Jackman, C. M., et al. (2014), Large-scale structure and dynamics of the magnetotails of Mercury, Earth, Jupiter and Saturn, *Space Sci. Rev.*, *182*, 85–154, doi:10.1007/s11214-014-0060-8.

Kalegaev, V. V., I. I. Alexeev, I. S. Nazarkov, V. Angelopoulos, and A. Runov (2014), On the large-scale structure of the tail current as measured by THEMIS, *Adv. Space Res.*, *54*(9), 1773–1785 ISSN 0273-1177, doi:10.1016/j.asr.2014.07.019.

Kistler, L. M., et al. (2005), Contribution of nonadiabatic ions to the cross-tail current in an O^+ dominated thin current sheet, *J. Geophys. Res.*, *110*, A06213, doi:10.1029/2004JA010653.

Korth, H., N. A. Tsyganenko, C. L. Johnson, L. C. Philpott, B. J. Anderson, M. M. Al Asad, S. C. Solomon, and R. L. McNuttJr (2015), Modular model for Mercury's magnetospheric magnetic field confined within the average observed magnetopause, *J. Geophys. Res. Space Physics*, *120*, 4503–4518, doi:10.1002/2015JA021022.

Imber, S. M., J. A. Slavin, H. U. Auster, and V. Angelopoulos (2011), A THEMIS survey of flux ropes and traveling compression regions: Location of the near-Earth reconnection site during solar minimum, *J. Geophys. Res.*, *116*, A02201, doi:10.1029/2010JA016026.

Imber, S. M., J. A. Slavin, S. A. Boardsen, B. J. Anderson, H. Korth, R. L. McNutt Jr., and S. C. Solomon (2014), MESSENGER observations of large dayside flux transfer events: Do they drive Mercury's substorm cycle?, *J. Geophys. Res. Space Physics*, *119*, 5613–5623, doi:10.1002/2014JA019884.

Jia, X., J. A. Slavin, T. I. Gombosi, L. K. S. Daldorff, G. Toth, and B. van der Holst (2015), Global MHD simulations of Mercury's magnetosphere with coupled planetary interior: Induction effect of the planetary conducting core on the global interaction, *J. Geophys. Res. Space Physics*, *120*, 4763–4775, doi:10.1002/2015JA021143.

Johnson, C. L., et al. (2012), MESSENGER observations of Mercury's magnetic field structure, *J. Geophys. Res.*, *117*, E00L14, doi:10.1029/2012JE004217.

Nagai, T., and S. Machida (1998), Magnetic reconnection in the near-earth magnetotail, in *New Perspectives on the Earth's Magnetotail*, edited by A. Nishida, D. N. Baker, and S. W. H. Cowley, AGU, Washington, D. C., doi: 10.1029/GM105p0211.

Nakai, H., Y. Kamide, and C. T. Russell (1999), Dependence of the near-Earth magnetotail magnetic field on storm and substorm activities, *J. Geophys. Res.*, *104*, 22,701–22,711, doi:10.1029/1999JA900273.

Nakamura, R., et al. (2002), Fast flow during current sheet thinning, *Geophys. Res. Lett.*, *29*(23), 2140, doi:10.1029/2002GL016200.

Narita, Y., R. Nakamura, and W. Baumjohann (2013), Cluster as current sheet surveyor in the magnetotail, *Ann. Geophys.*, *31*, 1605–1610, doi:10.5194/angeo-31-1605-2013.

Ogilvie, K. W., J. D. Scudder, V. M. Vasyliunas, R. E. Hartle, and G. L. Siscoe (1977), Observations at the planet Mercury by the plasma electron experiment: Mariner 10, *J. Geophys. Res.*, *82*, 1807–1824, doi:10.1029/JA082i013p01807.

Raines, J. M., J. A. Slavin, T. H. Zurbuchen, G. Gloeckler, B. J. Anderson, D. N. Baker, H. Korth, S. M. Krimigis, and R. L. McNutt Jr. (2011), MESSENGER observations of the plasma environment near Mercury, *Planet. Space Sci.*, *59*, 2004–2015, doi:10.1016/j.pss.2011.02.004.

Rich, F. J., V. M. Vasyliunas, and R. A. Wolf (1972), On the balance of stresses in the plasma sheet, *J. Geophys. Res.*, *77*, 4670–4676, doi:10.1029/JA077i025p04670.

Sharma, A. S., et al. (2008), Transient and localized processes in the magnetotail: A review, *Ann. Geophys.*, *26*, 955–1006.

Slavin, J. A., and R. E. Holzer (1979), The effect of erosion on the solar wind stand-off distance at Mercury, *J. Geophys. Res.*, *84*, 2076–2082, doi:10.1029/JA084iA05p02076.

Slavin, J. A., E. J. Smith, D. G. Sibeck, D. N. Baker, R. D. Zwickl, and S.-I. Akasofu (1985), An ISEE-3 study of average and substorm conditions in the distant magnetotail, *J. Geophys. Res.*, *90*, 10,875–10,895, doi:10.1029/JA090iA11p10875.

Slavin, J. A., et al. (2009), MESSENGER observations of magnetic reconnection in Mercury's magnetosphere, *Science*, *324*, 606–610, doi:10.1126/science.1172011.

Slavin, J. A., et al. (2010), MESSENGER observations of extreme loading and unloading of Mercury's magnetic tail, *Science*, *329*, 665–668, doi:10.1126/science.1188067.

Slavin, J. A., et al. (2012a), MESSENGER and Mariner 10 flyby observations of magnetotail structure and dynamics at Mercury, *J. Geophys. Res.*, *117*, A01215, doi:10.1029/2011JA016900.

Slavin, J. A., et al. (2012b), MESSENGER observations of a flux-transfer-event shower at Mercury, *J. Geophys. Res.*, *117*, A00M06, doi:10.1029/2012JA017926.

Sun, W.-J., et al. (2015), MESSENGER observations of magnetospheric substorm activity in Mercury's near magnetotail, *Geophys. Res. Lett.*, *42*, 3692–3699, doi:10.1002/2015GL064052.

Sun, W. J., S. Y. Fu, J. A. Slavin, J. M. Raines, Q. G. Zong, G. K. Poh, and T. H. Zurbuchen (2016), Spatial distribution of Mercury's flux ropes and reconnection fronts: MESSENGER observations, *J. Geophys. Res. Space Physics*, *121*, doi:10.1002/2016JA022787.

Sundberg, T., et al. (2012), MESSENGER observations of dipolarization events in Mercury's magnetotail, *J. Geophys. Res.*, *117*, A00M03, doi:10.1029/2012JA017756.

Trávníček, P. M., P. Hellinger, D. Schriver, D. Herčík, J. A. Slavin, and B. J. Anderson (2009), Kinetic instabilities in Mercury's magnetosphere: Three-dimensional simulation results, *Geophys. Res. Lett.*, *36*, L07104, doi:10.1029/2008GL036630.

Tsyganenko, N. A., and D. P. Stern (1996), Modeling the global magnetic field of the large-scale Birkeland current systems, *J. Geophys. Res.*, *101*, 27,187–27,198, doi:10.1029/96JA02735.

Volwerk, M., N. Andre, C. S. Arridge, C. M. Jackman, X. Jia, S. E. Milan, and A. Radioti (2013), Comparative magnetotail flapping: An overview of selected events at Earth, Jupiter and Saturn, *Ann. Geophys.*, *31*, 817–833, doi:10.5194/angeo-31-817-2013.

Wang, C.-P., L. R. Lyons, M. W. Chen, and F. R. Toffoletto (2004), Modeling the transition of the inner plasma sheet from weak to enhanced convection, *J. Geophys. Res.*, *109*, A12202, doi:10.1029/2004JA010591.

Winslow, R. M., B. J. Anderson, C. L. Johnson, J. A. Slavin, H. Korth, M. E. Purucker, D. N. Baker, and S. C. Solomon (2013), Mercury's magnetopause and bow shock from MESSENGER Magnetometer observations, *J. Geophys. Res. Space Physics*, *118*, 2213–2227, doi:10.1002/jgra.50237.